

# TOPOLOGICAL BIOMARKERS FOR REAL-TIME DETECTION OF EPILEPTIC SEIZURES

XIMENA FERNÁNDEZ AND DIEGO MATEOS

**ABSTRACT.** Automated seizure detection is a fundamental problem in computational neuroscience towards diagnosis and treatment's improvement of epileptic disease. We propose a real-time computational method for automated tracking and detection of epileptic seizures from raw neurophysiological recordings. Our mechanism is based on the topological analysis of the sliding-window embedding of the time series derived from simultaneously recorded channels. We extract topological biomarkers from the signals via the computation of the persistent homology of time-evolving topological spaces. Remarkably, the proposed biomarkers robustly captures the change in the brain dynamics during the ictal state. We apply our methods in different types of signals including scalp and intracranial EEG and MEG, in patients during interictal and ictal states, showing high accuracy in a range of clinical situations.

## 1. INTRODUCTION

Epilepsy is the second most common neurological disorder—behind strokes—that affects approximately fifty million people, according to the World Health Organization [29]. It is characterized by the occurrence of spontaneous seizures, which arise when large regions of the brain have synchronized neural activity and abnormally enhanced neuronal excitability. Understanding the mechanism that underlies the transition from a normal state to epileptic activity is of paramount importance for the diagnosis and treatment of epilepsy given that around a third of epilepsy patients are drug resistant.

In practice, epilepsy diagnosis is often performed by skilled neurophysiologists, who monitor the brain activity signal via electroencephalograms (EEG) or magnetoencephalograms (MEG) [31]. More efficient methods for seizure detection involve the automatic classification of the signals into preictal and ictal states (meaning before and during the seizure respectively) via pre-trained machine learning algorithms [43, 48]. Such algorithms require a preprocessing procedure of the whole signals for the feature extraction and, hence, are not likely to be applied for real-time seizure detection.

Although there is a wide variety of pathologies, conditions and network reorganizations that may result in epilepsy, there is a crucial observation towards its detection: the physiological signature of different seizures presents remarkable similarities from case to case. Concretely, a number of complex morphological patterns can be identified at a seizure-onset when monitoring the brain activity signal [34]. However, such patterns are hard to universally identify only from the raw signals given the high variance in the type of signal resultant from the recording method, and the particular physiological characteristics of each patient.

Epileptic seizures and more generally, brain dynamics, can be interpreted from the viewpoint of nonlinear dynamical systems [18, 21]. Indeed, Hodgkin and Huxley, awarded with the Nobel Prize in 1963, showed that the neuron activity can be modeled by a set of

nonlinear differential equations [20]. This discovery is especially relevant when studying epileptic seizures, since they are characterized by a synchronization in the brain network that replaces the usual complex nature of the neuronal activity, closer to chaotic behaviour.

In practice, the underlying equations describing the dynamical systems in study are not available. Hence, dynamics are often analyzed by studying the topology of their *attractors*; i.e., invariant subsets of the phase space towards which the system tends to evolve [5, 41, 15]. In our case, EEG and MEG signals represent the measurement of (certain functions of) some variables associated to the underlying (unknown) neural dynamical system. Its simultaneous embedding in a high dimensional Euclidean space represents a trajectory in the state space that approximates the associated attractor. The invariance of dynamical properties in most spontaneous and evoked seizures across brain regions and species [34] suggests the existence of particular *intrinsic* geometric properties in the embedding of the neurophysiological signals that should be analyzed.

Recently, the use of algebraic topology has had a striking success in the analysis of a wide variety of unstructured data. Topological Data Analysis (TDA) has emerged as a new mathematical field aiming to provide well-founded algebraic, statistical and algorithmic methods to infer, analyze and exploit the complex topological and geometric structures underlying raw data. Persistent homology [14], the vanguard technique in TDA, has shown successful results in the analysis and development of new theories in an increasing number of scientific fields such as medicine [28], biology [46], genomics [37], physics [8], chemistry [23], amongst others. In the particular field of multivariate time series analysis, information about quasi-periodic patterns and changes in the dynamics can be robustly detected in terms of the (persistent) homology of the embeddings [33, 32, 13]. Some initial works towards the application of topological invariants for the detection of epileptic signals have been developed in [36, 25]. However, these methods require complex preprocessing steps of the whole data, and they are not applicable to a real-time analysis of raw neurophysiological signals.

In this work, we propose a novel computational technique for the real-time tracking and detection of epileptic seizures from raw neurophysiological recordings. The key of our method is the identification of topological biomarkers that successfully capture the changes in the brain dynamics associated to epilepsy. The time-evolving behaviour of brain activity is geometrically encoded in terms of the *sliding-window embedding* of the multivariate time series derived from the simultaneously recorded channels. We extract topological features from the signals via the computation of the persistent homology of the time-varying point clouds obtained from the sequential embeddings in a high dimensional Euclidean space. The evolution of the dynamics is represented in a path of persistence diagrams—the output of persistent homology calculation—whose approximate first derivative quantifies the different states of the brain activity (c.f. [13, Section 4]). Concretely, the values of the first derivative are in correspondence with the amount of change in the global neural activity, where high values indicate the start and end points of an epileptic seizure. The same procedure applied to a discriminative sliding-window embedding for each channel (using Takens delay embedding’s theory [42]) may capture the specific channel(s) where the seizure starts and/or generalizes (see Figure 1). We also show that the *total persistence* [40]—a numerical topological summary computed from persistence diagrams—is sensitive to the presence of an epileptic seizure. This approach provides a scalable computational procedure to track the simultaneous evolution of raw neurophysiological recordings in real-time, that is robust to noise due to the *stability* property of persistent homology [6]. We present the

results of our methods in patients under a wide range of clinical situations—from focal to global seizures—and types of neurophysiological data—from scalp and intracranial EEG to MEG—. Remarkably, we obtain high accuracy in detection of ictal states over the different conditions, showing a robust mechanism for detection of the intrinsic signature present in seizure dynamic.

2. MATERIALS AND METHODS

**2.1. Topological analysis of time series.** Let  $\varphi_1, \varphi_2, \dots, \varphi_n : [0, T] \rightarrow \mathbb{R}$  be a collection of real-valued time series, such as multichannel EEG and MEG recordings. We will assume that the time series  $\{\varphi_i\}_{1 \leq i \leq n}$  are the result of observation functions applied to an underlying dynamical system. Namely, we assume that there exist a global continuous-time dynamical system  $(X, \phi)$  (where  $X$  is the phase space and  $\phi: \mathbb{R} \times X \rightarrow X$  is the evolution function), observation maps  $\{F_i : X \rightarrow \mathbb{R}\}_{1 \leq i \leq n}$  and an initial state  $x \in X$  that produce the time series

$$\begin{aligned} \varphi_i &: \mathbb{R} \rightarrow \mathbb{R} \\ t &\mapsto F_i(\phi(t, x)) \end{aligned}$$

for all  $1 \leq i \leq n$ .

We will analyze the underlying (unknown) dynamical system by studying the topology of their attractors [1, 2, 41, 42, 45].

In practice, we estimate the attractor  $M$  towards which the system is converging as the embedding of the time series  $\varphi = \{\varphi_i\}_{1 \leq i \leq n}$  in  $\mathbb{R}^n$ , defined as

$$E_\varphi = \{(\varphi_1(t), \varphi_2(t), \dots, \varphi_n(t)) : t \in [0, T]\}.$$

**2.2. Sliding-Window Embedding.** Epileptic seizures are characterized by the abrupt switching between different states in the brain dynamics. Such transitions are reflected in changes in the topology of the local embeddings of the dynamic observations. Given a collection of real-valued time series  $\varphi = \{\varphi_i\}_{1 \leq i \leq n}$  and a window-size  $0 < w \leq T$ , we define the *sliding-window embedding* at  $t \in [w, T]$  as the subset of  $\mathbb{R}^n$  given by

$$\text{SWE}_{\varphi, w}(t) = \{(\varphi_1(s), \varphi_2(s), \dots, \varphi_n(s)) : s \in [t - w, t]\}.$$

This procedure describes a path of time-evolving topological spaces

$$\begin{aligned} [w, T] &\rightarrow \text{Top} \\ t &\mapsto \text{SWE}_{\varphi, w}(t). \end{aligned}$$

Notice that, in practical applications, the signals are only recorded at a finite set of equidistant sample times  $t_1, t_2, \dots, t_m \in [0, T]$ . Hence, the topological spaces  $\text{SWE}_{\varphi, w}(t)$  are described by just a finite sample of its points. Computational methods for the inference of topological invariants from point clouds, such as *persistence homology*, will be then employed.

**2.3. Persistent Homology.** One of the best known computable invariants in algebraic topology is *homology* [19]. This invariant assigns to every topological space  $X$  a sequence  $H_i(X)$  of groups that captures geometric signatures at dimension  $i$ . Indeed, the rank of the group  $H_i(X)$  defines the *i-th Betti number*  $\beta_i$  of  $X$  and it quantifies the number of (independent)  $i$ -dimensional holes existing in  $X$ . For instance,  $\beta_0$  represents the number of connected components,  $\beta_1$  the number of 1-dimensional cycles,  $\beta_2$  the number of voids and so on. There exist efficient algorithms—based on normal matrix decompositions—to

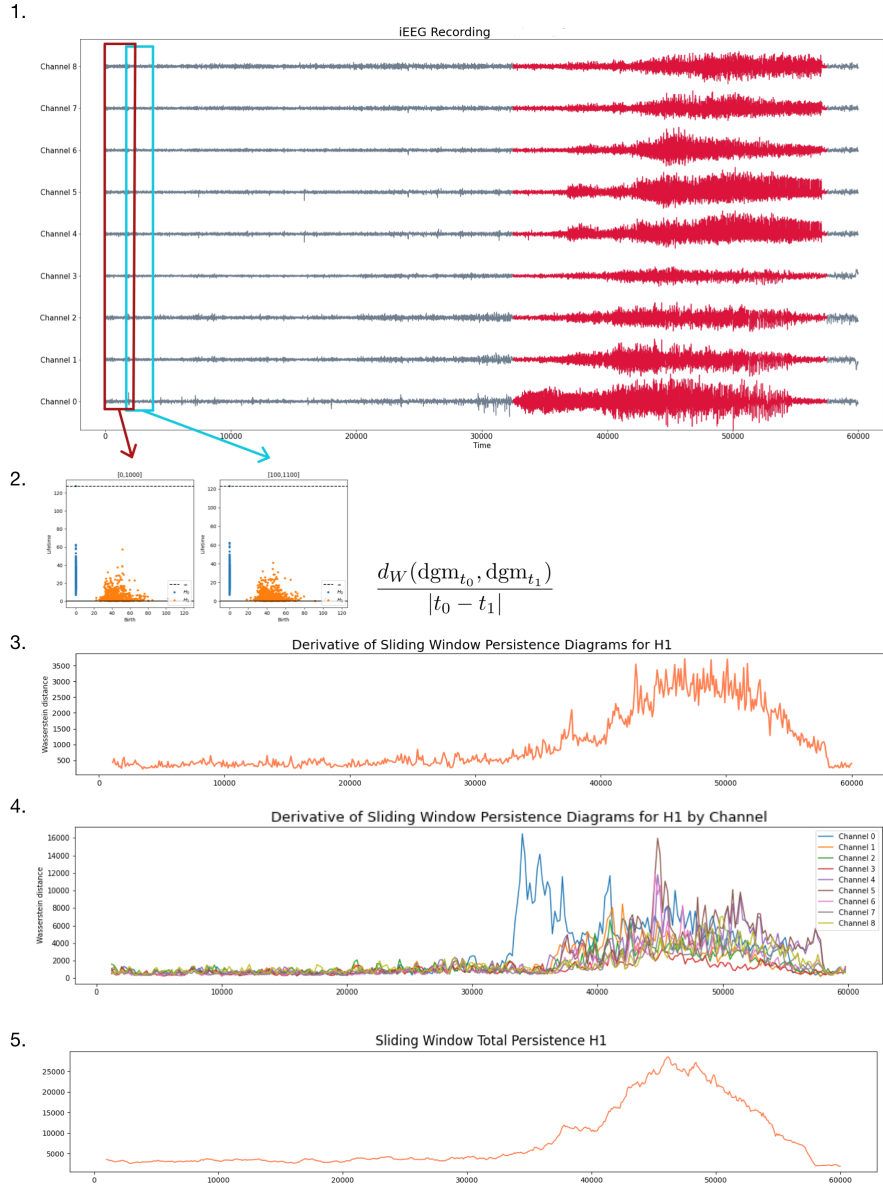


FIGURE 1. **Pipeline of the topological analysis of a raw physiological recording of an epileptic seizure.** **1.** Recording of neural activity by an iEEG with 9 channels (200 Hz of sampling rate). The epileptic seizure starts in a few channels and it generalizes by the end of the recording (where the patient loses his consciousness). The ictal state is marked in red. **2.** The sliding-window embedding of the signals determine a path of time-evolving persistence diagrams. **3.** The approximate of the first derivative of persistence diagrams at degree 1 for the joint set of signals. **4.** The approximate of the first derivative of persistence diagrams at degree 1, when the embedding is performed individually by channel using Takens' delay embedding. **5.** The total persistence biomarker for  $H_1$ .

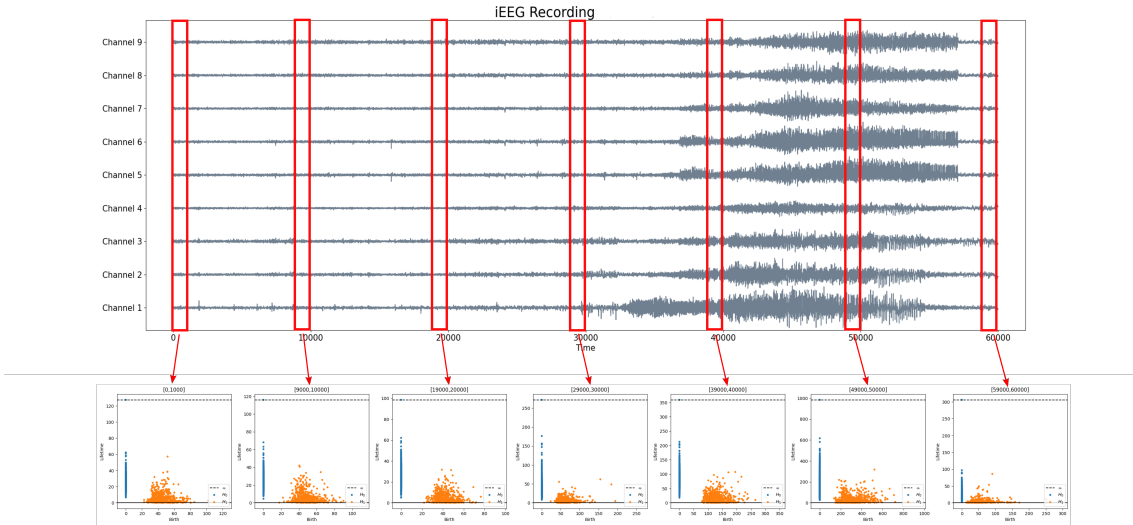


FIGURE 2. Path of persistent diagrams associated to the time evolving sliding-window embeddings  $SWE_{\varphi,w}(t)$ .

compute homology from the combinatorial descriptions of topological spaces. Among the most used discrete representations are the *simplicial complexes*, structures composed by simplices of different dimension (such as points, edges, triangles, etc) that encode all the relevant the topological information of a space (for instance, a sphere can be codified as the boundary of a tetrahedron).

When analysing data, the topological space is often described through a finite sample of its points. In that case, the standard algorithm to compute homology is unable to recover any relevant property of the topology of the underlying structure, since it literally interprets the input as a finite discrete set. Persistent homology overcomes this limitation by looking at the sample at different scales of spatial resolution. More concretely, this computational method quantifies the evolution of homology groups of the point cloud when replacing each point by a ball of common increasing radius. Given a point cloud  $X_n$  of size  $n$  embedded in a Euclidean space, the *Vietoris-Rips complex*  $VR_\epsilon$  at scale  $\epsilon > 0$  is a simplicial complex with a simplex of dimension  $m$  of for every subset of data points  $\{x_0, x_1, \dots, x_m\}$  at pairwise distances less than  $\epsilon$ . Geometrically,  $VR_\epsilon$  is built as follows. Construct a ball of radius  $\epsilon/2$  with center on each data point. Then, put an edge joining the center of every pair of intersecting balls. Finally, every time there is a subset of  $m+1$  points pairwise connected with edges, then fill with the convex hull of the points in  $\mathbb{R}^{2m+1}$  (these are the  $m$ -simplices) (see Figure 3). Notice that if  $\epsilon < \epsilon'$ , then  $VR_\epsilon \subseteq VR_{\epsilon'}$ . So  $\{VR_\epsilon\}_{\epsilon>0}$  represents a filtration of simplicial complexes whose homology groups capture the evolution of the topology of the point cloud for different resolution scales. The persistent homology of  $X_n$  at degree  $i$  is the family of homology groups  $\{H_i(VR_\epsilon)\}_{\epsilon>0}$ , along with the induced maps  $H_i(VR_\epsilon) \rightarrow H_i(VR_{\epsilon'})$  every time  $\epsilon < \epsilon'$ . All this information can be summarized as the list of parameter scales at which every generator in homology appears (birth) and disappears (death). This suggests a graphical representation of persistent homology as a diagram called *persistence diagram* that represents every generator as a two-coordinated

point whose first coordinate means its birth and the second coordinate, its death. For technical reasons, the diagonal (with generators with the same birth as death) will also be considered as part of every persistence diagram, with infinite multiplicity.

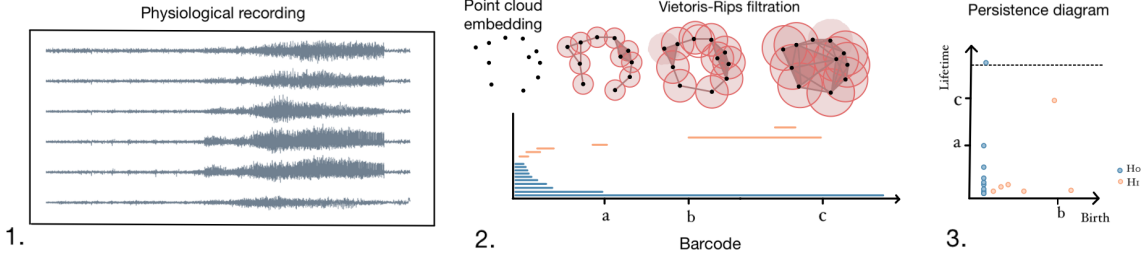


FIGURE 3. **Persistent Homology Pipeline.** **1.** Multivariate signals derived from the physiological recording. **2.** Point cloud embedding of the signals and the Vietoris-Rips filtration (top). Barcode description of the persistent homology (bottom). **3.** Persistence diagram. Every point represents a generator in homology, the first coordinate represents its birth and the second coordinate, its lifetime.

Similarity and differences in the topological signatures captured by persistence diagrams can be measured, e.g. with the Wasserstein distance. Given  $\mathcal{D}$  and  $\mathcal{D}'$  persistence diagrams and  $p \geq 1$ , its  $p$ -Wasserstein distance  $d_{W,p}$  is defined as

$$d_{W,p}(\mathcal{D}, \mathcal{D}') = \inf_{\psi: \mathcal{D} \rightarrow \mathcal{D}'} \left( \sum_{(x,y) \in \mathcal{D}} \|(x,y) - \psi(x,y)\|_{\infty}^p \right)^{1/p}$$

where the infimum is taken over all bijections  $\psi$  between generators in  $\text{dgm}$  and  $\text{dgm}'$  with finite death. The Wasserstein distance only captures the fundamental differences in the underlying topology of point clouds, whereas small changes in the input data are quantified as only a small change in the associated persistence diagram [11]. This property of persistent homology is known as *stability*, and makes it a useful tool for dealing with real-world, noisy data.

**2.4. Topological summaries.** Let  $\varphi = \{\varphi_i\}_{1 \leq i \leq n}$  be a collection of real-valued time series on  $[0, T]$  and let  $w$  be the window size. We capture information of the evolution of the topology of the sliding-window embedding  $\text{SWE}_{\varphi,w}(t_j)$  using persistent homology. Concretely, we consider the path of time-varying persistence diagrams

$$(1) \quad \begin{aligned} [w, T] &\rightarrow \text{Dgm} \\ t &\mapsto \text{dgm}(\text{SWE}_{\varphi,w}(t)). \end{aligned}$$

In practice, we have  $\{t_j\}_{1 \leq j \leq m}$  be a finite sample of equidistant times and set  $0 < w \leq T$  as a multiple of  $t_j - t_{j-1}$ . In order to quantify the local changes in the topology of the embedding along the time interval, we estimate the *first order derivative* of the map (1) as

$$(2) \quad \frac{d_{W,p}(\text{dgm}(\text{SWE}_{\varphi,w}(t_j)), \text{dgm}(\text{SWE}_{\varphi,w}(t_{j-1})))}{t_j - t_{j-1}}$$

for every  $1 \leq j \leq m - 1$ .

We will also associate to every diagram  $\text{dgm}(\text{SWE}_{\varphi,w}(t_j))$ ,  $1 \leq j \leq m$ , a measure of its *topological complexity*. Given  $\mathcal{D}$  a persistence diagram, the *persistence* of a generator  $(x, y) \in \mathcal{D}$  with finite death is  $\text{pers}(x, y) := y - x$ . For  $k \geq 1$ , the *k-total persistence* of  $\mathcal{D}$  [7] is defined as

$$\text{Pers}_k(\mathcal{D}) = \sum_{(x,y) \in \mathcal{D}} \text{pers}(x, y)^k.$$

**2.5. Data.** In this study, we have analyzed two different databases. The first database was prepared by the Toronto Western Hospital, Canada, and it contains both intracranial EEG (iEEG) and MEG recordings from four patients with a wide range of clinical situations. This data from Patient 1 was previously analyzed in [44], while Patients 2-4 were investigated in [10].

- **Patient 1.** It presents a medically refractory temporal lobe epilepsy. The iEEG recording was obtained as part of the patient’s routine clinical presurgical analysis. The electrodes were positioned in a number of locations including the amygdala and hippocampal structures of both temporal lobes. The data consists of 300 seconds of recording from 19 channels at 200 Hz sampling rate.
- **Patient 2.** It presents a symptomatic (formerly known as secondary) generalized epilepsy. The data consists of a MEG recording of 120 seconds from 171 channels at 625 Hz sampling rate. The recording sensors covered the whole cerebral cortex.
- **Patient 3.** It presents a primary generalized absence epilepsy. The data consists of a MEG recording of 120 seconds from 144 channels at 625 Hz sampling rate. The recording sensors also covered the whole cerebral cortex. The recording sensors also covered the whole cerebral cortex.
- **Patient 4.** It has a frontal lobe epilepsy with a right frontal subcortical *heterotopia* (a form of cortical dysplasia). The data consists of a MEG recording of 120 seconds from 148 channels at 625 Hz sampling rate. The recording sensors also covered the whole cerebral cortex.

The second database is an open-source scalp EEG database CHB-MIT [17], provided by the Massachusetts Institute of Technology, USA. The recordings were collected from pediatric subjects with intractable seizures at the Children’s Hospital Boston. We selected for this exposition a particular patient that presents complex seizure information, which turned out to be hard to identify using standard methods.

- **Patient 5.** It corresponds to case *chb01* in the CHB-MIT database. The data consists of an EEG recording with 23 sensors at 256 Hz sampling frequency.

### 3. RESULTS

**3.1. Topological seizure detection.** In this section, we show how the topological biomarkers described at Subsection 2.4 can be used to consistently detect the ictal state. We present the topological analysis of the data described at Subsection 2.5. The window size  $w$  at the sliding-window embedding is set to a value equivalent to 1 second of recording for patients 2, 3 and 4 (with sampling rate 256 Hz) and 2 seconds for patients 1 and 5 (with sampling rate 200 Hz and 256 Hz respectively). For every case study, all the topological summaries are computed for degree 0 and 1. The computation of the approximation of the first derivative is performed using the Wasserstein distance for  $p = 1$ . The *k*-total

persistence is evaluated for  $k = 1$ . The finite sample of the time interval  $[0, T]$  for every recording is determined as evenly spaced times with a stride equivalent to 0.5 seconds.

3.1.1. *Results.* Patient 1 presents a focal seizure that rapidly generalizes (see Figure 4). This is reflected in a gradual increase in the value of all the topological indicators, specially the ones associated to persistent homology at degree 1. On the other hand, the continuous decrease in the biomarkers by the end of the ictal state reflects the progressive global desynchronization.

Patients 2 and 3 present a global seizure (see Figures 5 and 6). The onset is determined by a synchronized spike that triggers all the topological indicators, with an abrupt decrease after the seizure ends. The peaks in the first derivative at the start and end of the ictal state reveals abrupt changes in the dynamics, whereas low values in the interior of the ictal state indicate a stable global dynamic during the seizure (see Subsection 3.1.2 for details on the interpretability of every topological indicator).

Patient 4 presents a (focal) epileptic seizure in the frontotemporal area, that is evidenced in a change of dynamics in only a subset of the channels in the MEG recording (see Figure 7). As in the previous cases, there is a peak in the sliding-window derivatives for degree 0 and 1 at the beginning and end of the ictal state. However, this case presents a gradual decrease in the values of the derivative at the post ictal state, showing a slow return to baseline. A similar situation can be read from the total persistence indicators, which present an abrupt increase during the ictal state in a plateau shape, and gradual recovery to baseline state after the seizure.

Patient 5 presents a complex pattern during (and also after) the ictal state, that most of standard techniques for seizure detection are not able to recognize (see Subsection 3.2). Remarkably, all our topological indicators are triggered during the ictal interval, whereas they present stable low values at the preictal stage (see Figure 8). They also show a gradual decrease during the postictal stage.

3.1.2. *Interpretability of the topological biomarkers.* In this section, we offer a detailed description of the connection between the seizure dynamics encoded by the physiological signals and the topological summaries.

*Persistent homology at degree 0* quantifies the connectivity of the point cloud. Every point at the persistent diagram  $\mathcal{D}_0$  represents a generator (a connected component) that is born at the scale parameter  $\epsilon = 0$  and dies at the value of  $\epsilon > 0$  at which the connected component represented by the generator joins another one in the Vietoris-Rips filtration. In particular, there is always a single generator with infinite lifetime, indicating that the Vietoris-Rips complex for large values of  $\epsilon$  is connected. However, the persistence of the rest of the generators encodes relevant properties of the embedding of the signals. For instance, the persistence of the generator with maximum finite lifetime equals the diameter of the point cloud and, hence, it is correlated with the amplitude of the signals. Moreover, the variance of the values of the persistence of the generators in  $\mathcal{D}_0$  is associated with the density of sampling of the underlying geometric space. Given that the size of the point cloud remains constant along all the time-varying embeddings, the distribution of the persistence of generators in  $\mathcal{D}_0$  is related to the rate between amplitude (also spikes) and frequency, and the synchronization of the oscillations in all the signals simultaneously.

*Persistent homology at degree 1* summarizes data about the (independent) 1-dimensional cycles that can be reconstructed from the point cloud. Generators with long lifetime represent structural cycles in the embedding, whereas the ones with short lifetime are

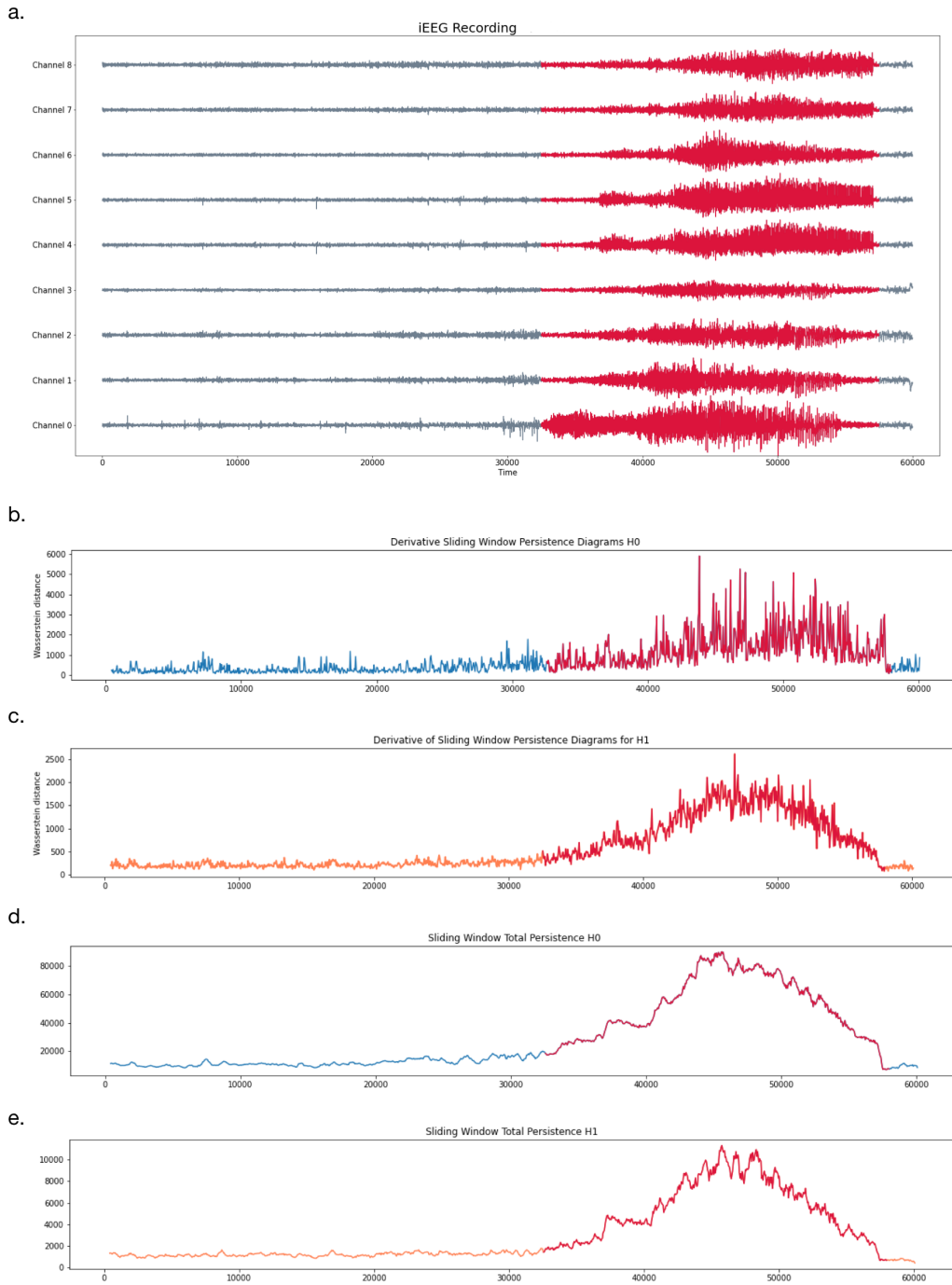


FIGURE 4. **Patient 1.** The total time-interval of the analysis is  $[0, 60000]$ , where the ictal state is at  $[32500, 58000]$  (in red). **a.** iEEG with 9 sensors at frequency 200 Hz. **b-c.** Estimator of first derivative of the time-evolving persistence diagrams for degrees 0 and 1. **d-e.** Total persistence for degrees 0 and 1.

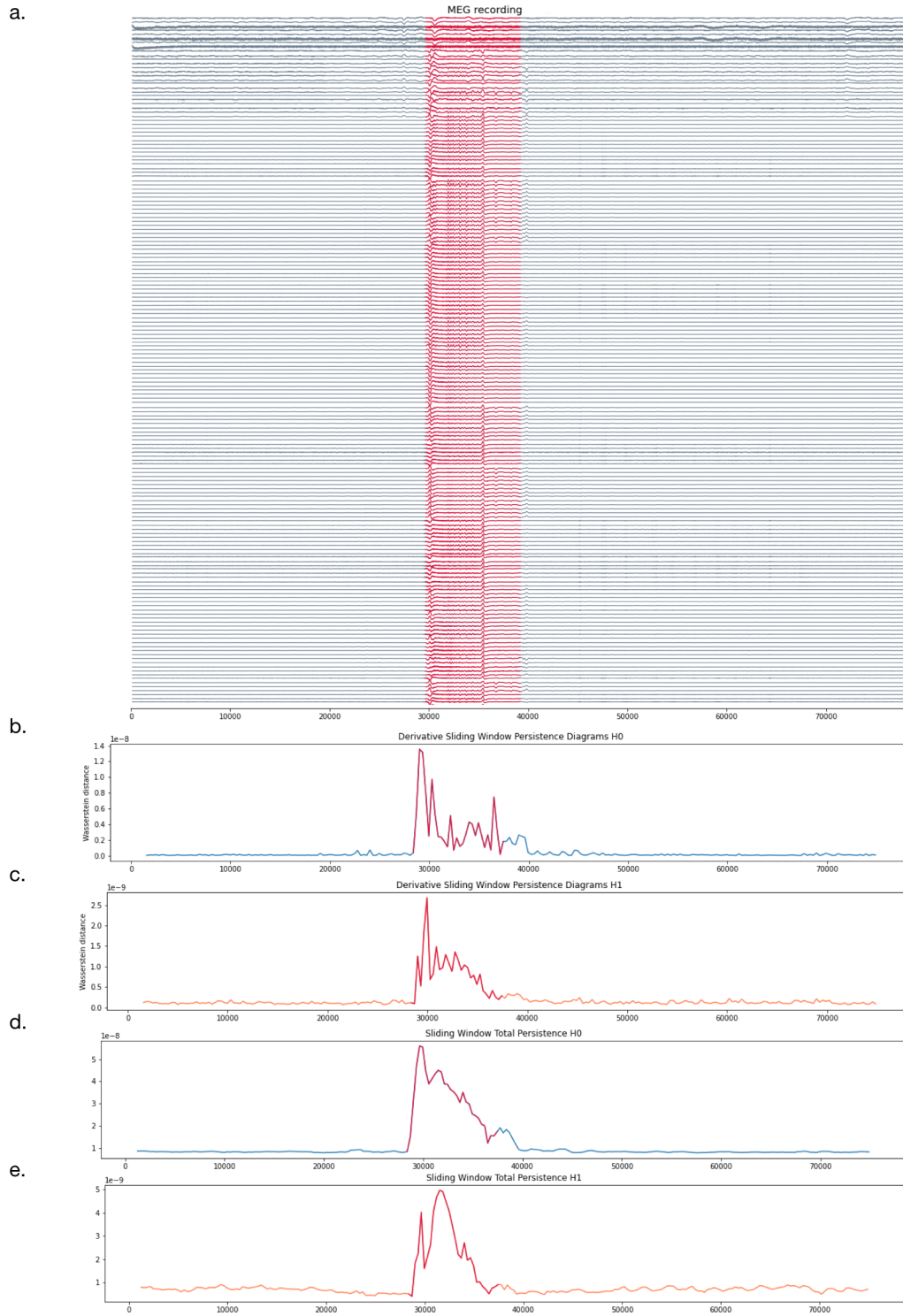


FIGURE 5. **Patient 2**. The total time-interval of the analysis is  $[0, 75000]$ , where the ictal state is at  $[28375, 37500]$  (in red). **a**. MEG with 171 sensors at frequency 625 Hz. **b-c**. Estimator of first derivative of the time-evolving persistence diagrams for degrees 0 and 1. **d-e**. Total persistence for degrees 0 and 1.

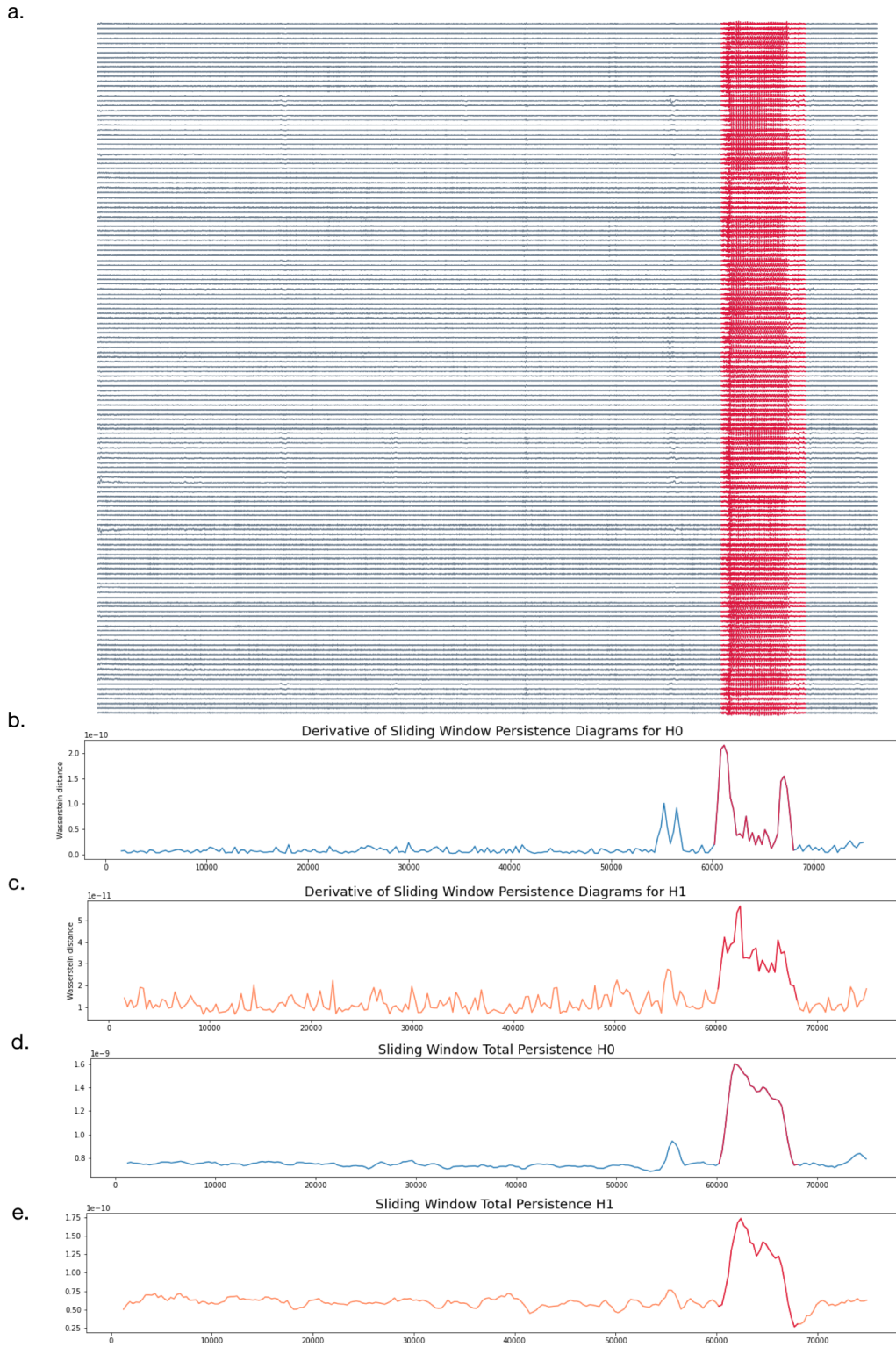


FIGURE 6. **Patient 3.** The total time-interval of the analysis is  $[0, 75000]$ , where the ictal state is at  $[60000, 68125]$  (in red). **a.** MEG with 141 sensors at frequency 625 Hz. **b-c.** Estimator of first derivative of the time-evolving persistence diagrams for degrees 0 and 1. **d-e.** Total persistence for degrees 0 and 1.



FIGURE 7. **Patient 4.** The total time-interval of the analysis is  $[0, 75000]$ , where the ictal state is at  $[58500, 68300]$  (in red). **a.** MEG with 148 sensors at frequency 625 Hz. **b-c.** Estimator of first derivative of the time-evolving persistence diagrams for degrees 0 and 1. **d-e.** Total persistence for degrees 0 and 1.

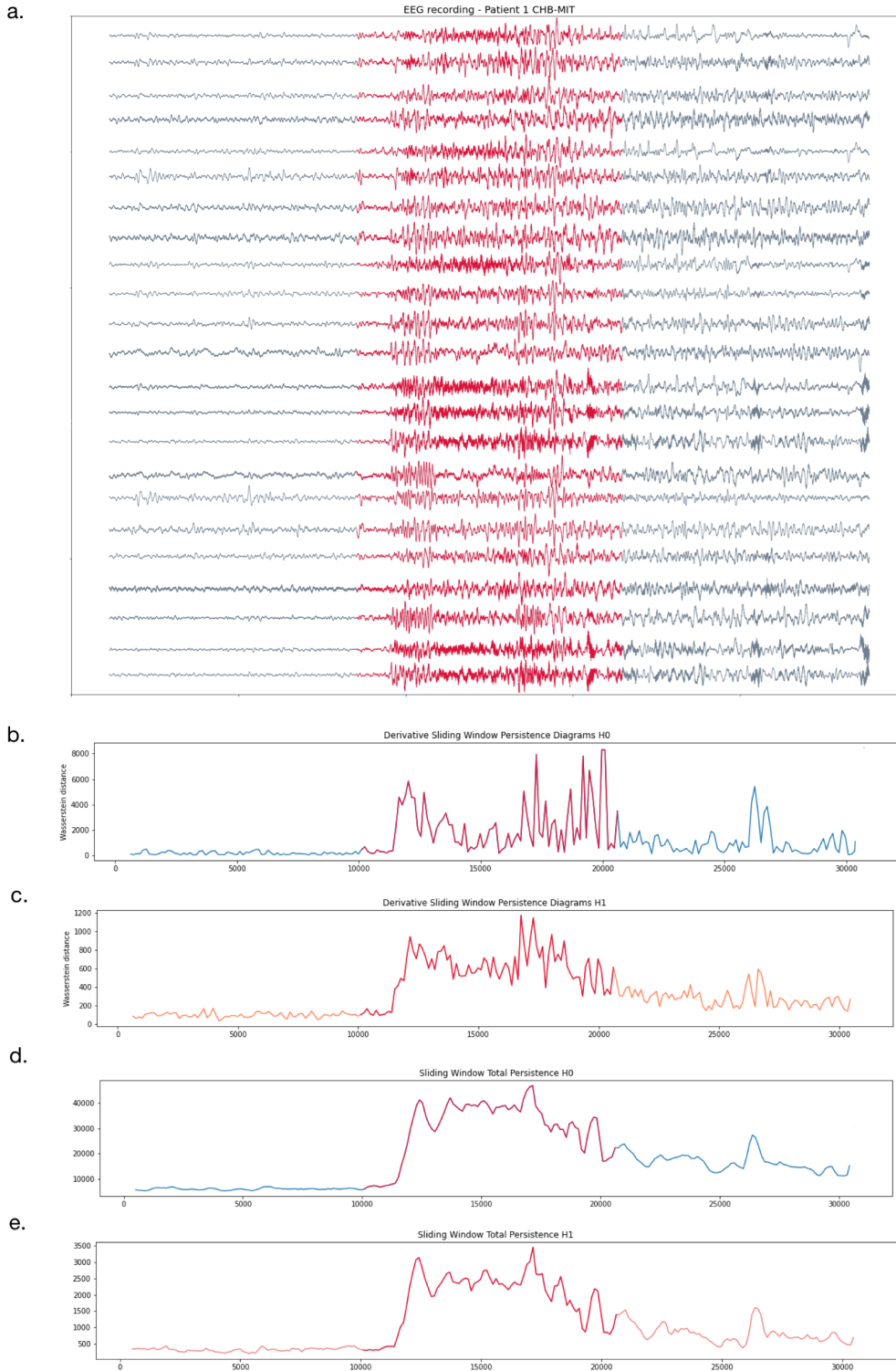


FIGURE 8. **Patient 5 (*chb01* from CHB-MIT database).** The total time-interval of the analysis is  $[0, 30723]$ , where the ictal state is at  $[10000, 20723]$  (in red). **a.** EEG with 23 sensors at frequency 256 Hz. **b-c.** Estimator of first derivative of the time-evolving persistence diagrams for degrees 0 and 1. **d-e.** Total persistence for degrees 0 and 1.

associated with small holes in areas of low density. At the signal level, homology at degree 1 of the embedding encodes the presence of synchronized (quasi) periodic patterns, while its persistence amounts to its level of synchronization and its amplitude.

The *estimator of the first derivative* of the persistence of the time-evolving point clouds measures the local changes in the geometry and topology of the embeddings. There is a number of situations quantified by this topological biomarker:

- abrupt change from low to high values of the derivative when the seizure starts and ends reflects a global change in the dynamics induced by a generalized seizure.
- progressive increasing values of the derivative from low to high the when the seizure starts and/or decreasing values when the seizure ends is an indicator of the starting of a focal seizure that generalizes by the end and, analogously, of brain activity that progressively desynchronizes by the end of the seizure.

Moreover, during the seizure the derivative might conserve high values (as at the start and end) or it might decrease the value of the highest peak (still having greater values that at the interictal state). This is consequence of the type of seizure pattern displayed at the ictal state:

- low values of the derivative after the seizure starts and before it ends means a consistent and uniform dynamic behaviour during the ictal state;
- high values of the derivative throughout the ictal state represents a non-stable seizure dynamic, in which there are constant changes in the amplitude and frequency, periodicity, spikes and wave activity [34].

The *total persistence* biomarker consists of a summary of the lifetime of the generators in the time-evolving persistence diagrams, for every degree. It quantifies numerically the complexity of the dynamics encoded in the time-evolving embeddings by means of its topological features. During the seizure, the total persistence for both degrees 0 and 1 is triggered, while it presents low values during the interictal state.

**3.1.3. Computational complexity.** The *standard algorithm* used to compute persistent homology was first introduced in [12] and it is based on the Gaussian reduction of the boundary matrix. Persistent homology for degree up to  $k$  depends on the  $(k + 1)$ -skeleton of the filtration and the worst-case computational complexity is cubical in the number  $N$  of simplices of dimension at most  $k + 1$  [27, 30]. An alternative algorithm for the reduction of the boundary matrix, introduced in [26], has complexity  $O(N^\omega)$ , with  $\omega$  the matrix multiplication coefficient. At present, the best bound for  $\omega$  is 2.376 [9]. In practice, computation of persistent homology has lower complexity. For Vietoris–Rips filtrations, the worst case complexity is for  $k$ -dimensional persistent homology is  $O\left(\binom{n}{k+2}^3\right) = O(n^{3(k+2)})$  with  $n$  the number of vertices of  $\mathbb{X}_n$ . However, [16] proved that, for instance, the average complexity for the reduction of the boundary matrix of degree 1 is upper bounded by  $O(n^5 \log^2(n))$ . Moreover, they showed that this upper bound seems to be not tight, since experimental simulations show that the average cost of the reduction of the 1-boundary matrix follows a curve of around  $O(n^{3.73})$ .

Our approach consists of the real time computation of the persistent diagrams associated to the time-evolving point clouds of size equivalent to 500 points (625 points for MEG recordings at sampling frequency 625 Hz, 400 points for iEEG recordings at frequency 200 Hz and 512 points for EEG recordings at frequency 256 Hz). These diagrams are updated

every 0.5 seconds. The execution time of the computation of every diagram is  $\sim 0.25$  seconds<sup>1</sup> and it is performed with the software `Ripsler` [4].

The 1-Wasserstein distance between persistence diagrams can be computed using the Hungarian algorithm [22] in  $O(d^3)$  time, where  $d$  is the total number of points in the two diagrams. This algorithm is implemented in the package `Ripsler`, and in practice it takes  $\sim 0.1$  seconds.

The total persistence of a persistence diagram can be computed in linear time in the number of points of a diagram, which in practice takes only  $\sim 0.5 \times 10^{-5}$  seconds.

Overall, our pipeline consists of the computation of the persistence diagram up to degree 1 of the sliding-window embedding of the signals, and the computation of the derivative and the total persistence indicators for every degree. All this process (which is updated every 0.5 seconds) takes less than 0.5 seconds and it can be performed in real time.

**3.2. Comparison with standard seizure indicators.** There is a number of commonly used methods to analyze time series obtained from neurophysiological recordings, which are applied to study epilepsy. In this section, we analyze of our datasets with some of the most popular procedures for time series analysis.

One of the most standard techniques in signal processing is the *time-frequency analysis*, which inspects a signal in both time and frequency domains simultaneously. For instance, the *spectrogram* of a multichannel signal returns the Short-Time Fourier Transform (STFT) containing an estimate of the short-term time-localized frequency content. In our analysis, we computed the spectrogram of every recording using the method `signal.spectrogram` from the Python library `scipy` (see Figure 9). The STFT analysis for Patients 1-5 shows changes in the time-frequency data during the ictal state, but in general they are not sufficiently precise to determine the start and end of the seizure onset (with exception of Patient 3).

Another popular tool to quantify the uncertainty contained in time series data is the *Lempel-Ziv complexity (LZ)*. Concretely, the LZ-complexity measures how diverse are the patterns that are present in a particular signal. The LZ-method was introduced back in 1976 by Abraham Lempel and Jacob Ziv to study binary sequences [24]. This algorithm has been used to study EEG brain activity for more than 20 years, with some early studies focusing on epilepsy [38] and depth of anaesthesia [47], and more modern ones on other altered states of consciousness [39]. We study the average LZ-complexity using our own implementation in `Python` of the standard LZ-algorithm (see Figure 10). The LZ indicator shows an abrupt drop during the ictal state for Patients 2 and 3, whereas its behaviour is not an indicative of the seizure dynamics for the rest of the patients.

Finally, we consider a robust non-linear statistical measure to quantify the complexity of a dynamical system in terms of time series: the *permutation entropy*. This mechanism, introduced by Bandt and Pompe in 2002 [3], aims to capture the order relations between the values of a time series by extracting a probability distribution of the ordinal patterns and subsequently computing the Shannon entropy. In our analysis, we employed the method `permutation_entropy` from the Python library `ordpy` [35]. The PE measure shows an extraordinary performance in seizure detection for MEG recordings (Patients 2-4), but it does not show to be a good seizure indicative for iEEG and EEG recordings (Patient 1 and 5 respectively). See Figure 11.

---

<sup>1</sup>MacBook Pro 8-core CPU 32-core GPU 16 GB unified memory.

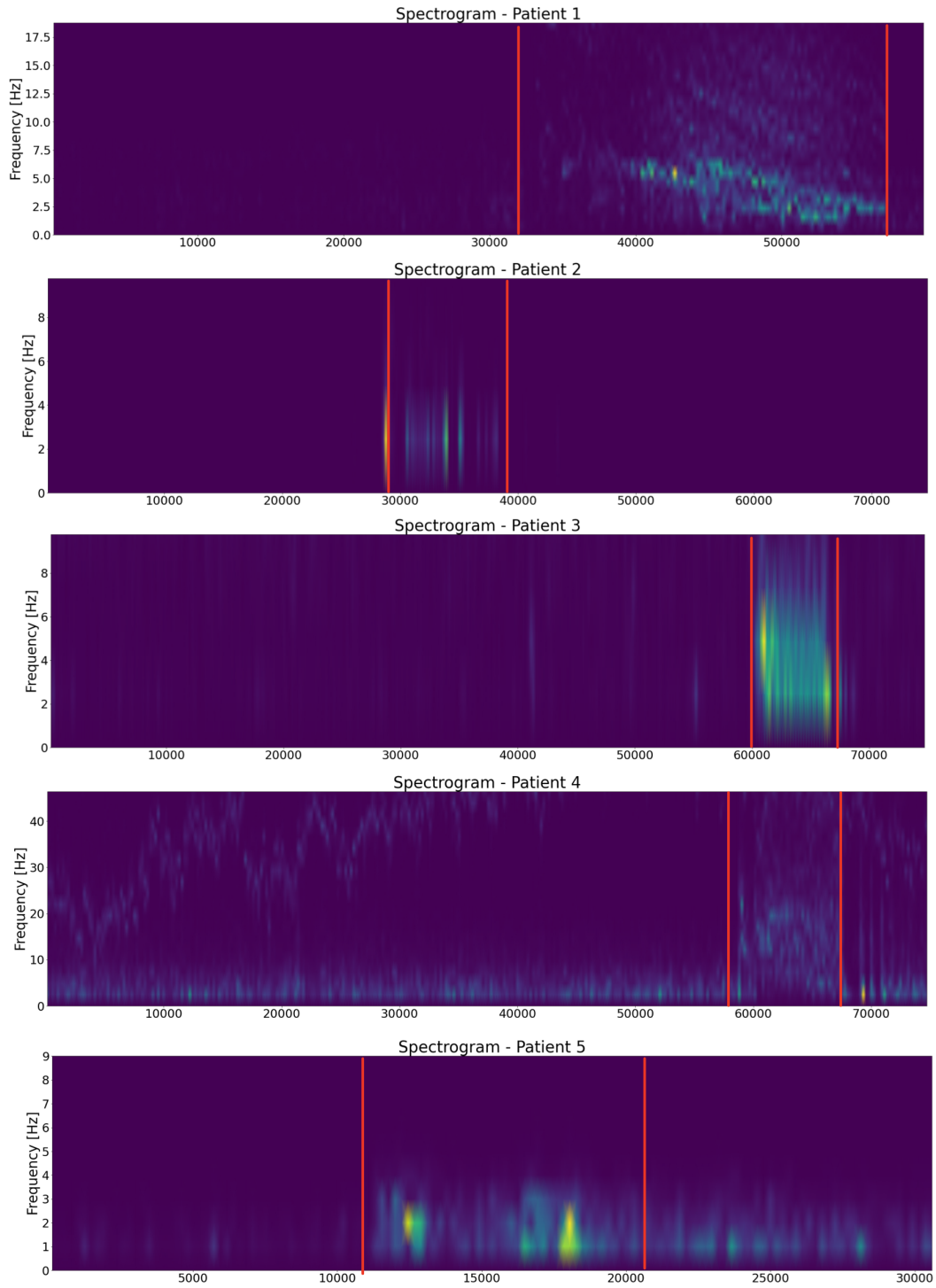


FIGURE 9. **Time-frequency analysis.** Spectrogram for Patients 1-5 (ictal state in red).

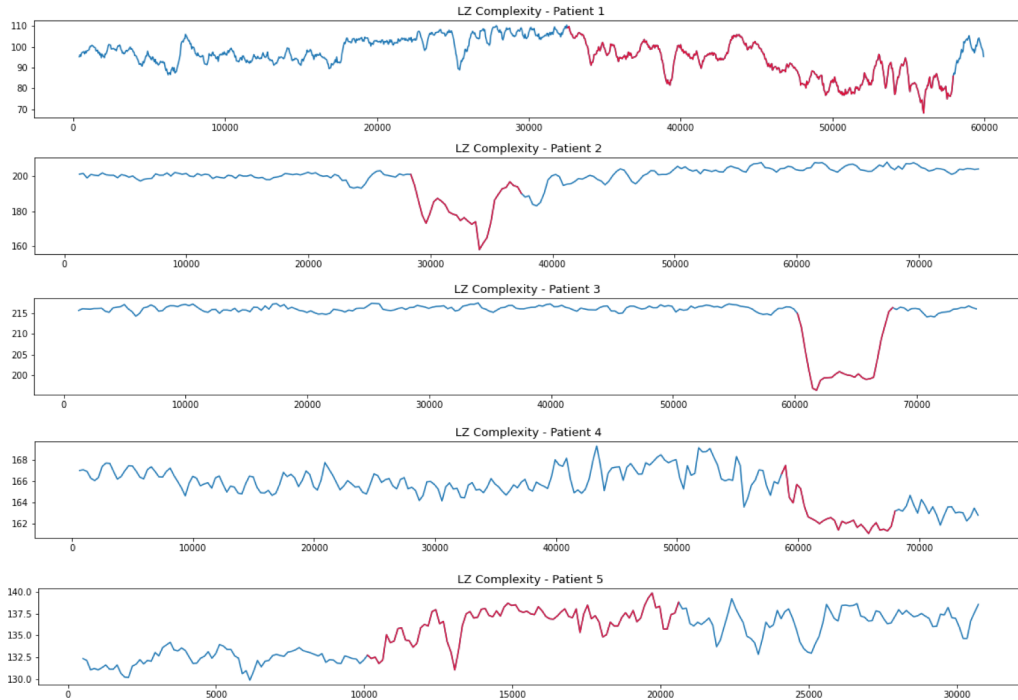


FIGURE 10. **LZ Complexity.** The average of the Lempel-Ziev complexity over all channels, for Patients 1-5 (ictal state in red).

**3.3. Local versus global seizures.** Epileptic seizures may involve either part of the cerebral hemisphere (*focal* seizures) or, on the contrary, the entire brain (*generalized* seizures)—the latter usually presenting loss of consciousness. This difference is reflected in either a local change in the brain dynamics, in which only a fraction of the set of the physiological signals presents a different behaviour, or a global change, in which all the signals present a synchronized seizure pattern.

Global versus local dynamics can be geometrically understood using algebraic and differential topology. Indeed, time-delay embeddings of scalar time-series data, introduced by Takens in the 80’s [42], is a well-known technique to recover the underlying global dynamics induced by a single observation. Concretely, Takens’ theorem gives conditions under which the topology of a smooth attractor can be reconstructed from a generic observable function, with dimensional bounds related to those of the Whitney Embedding Theorem. It implies in particular that if  $\varphi_i(t)$  is a real valued signal (for instance, one channel of the multichannel recording), then the *delay coordinate map*

$$t \mapsto \left( \varphi_i(t), \varphi_i(t + \tau), \varphi_i(t + 2\tau) \dots, \varphi_i(t + (D - 1)\tau) \right)$$

is an embedding of an orbit. Here  $D$  is the embedding dimension (theoretically representing the number of variables of the original system) and  $\tau$  is the time delay. If the attractor is a smooth manifold  $M$  of dimension  $d$ , under certain conditions Takens’ theorem implies that the delay embedding of the signal with  $D \geq 2d + 1$  is diffeomorphic to  $M$ .

Time-delay embeddings allow us to derive a technique to understand both focal and generalized seizures. Concretely, we analyze the dynamic induced by every individual signal from a multichannel electrophysiological recording and determine if they are consistent or

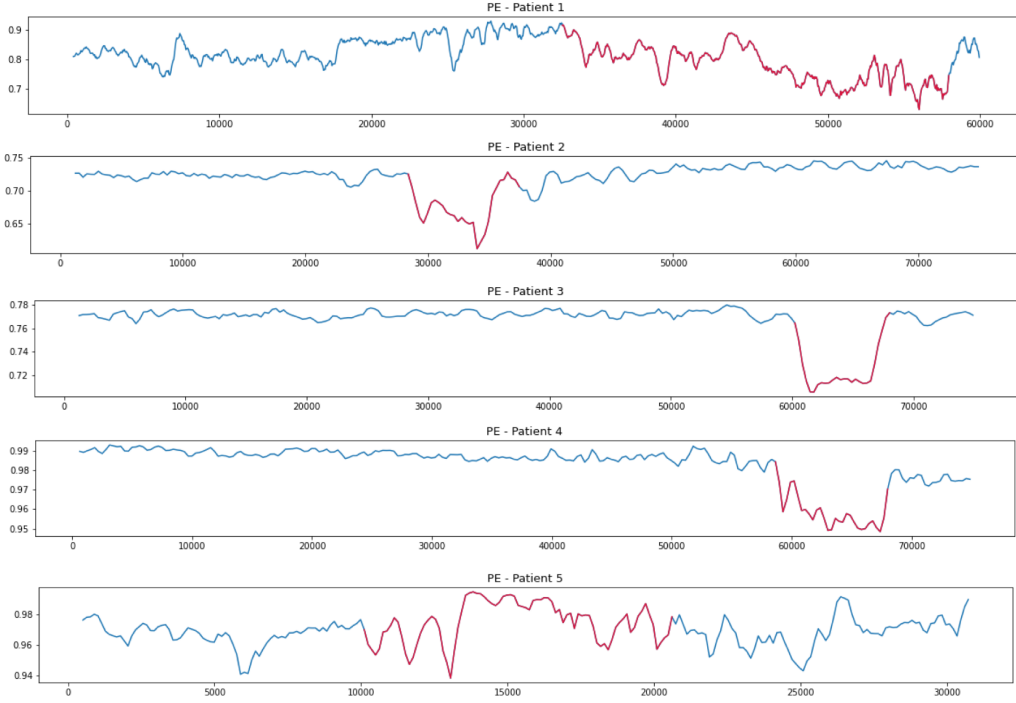


FIGURE 11. **Permutation Entropy.** The average of the PE indicator over all channels, for Patients 1-5 (ictal state in red).

not. For generalized seizures, the global dynamic induced by every channel should coincide, whereas for focal seizures different local dynamics may arise.

The procedure works as follows. For every signal  $\varphi_i$  ( $1 \leq i \leq n$ ) from the multichannel recording, compute the *sliding-window time-delay embedding* at  $t \in [w, T - (D - 1)\tau]$ , defined as the subset of  $\mathbb{R}^D$  given by

$$\text{SWE}_{\varphi_i, w}(t) = \{(\varphi_i(s), \varphi_i(s + \tau), \dots, \varphi_{D-1}(s + (D - 1)\tau)) : s \in [t - w, t]\}.$$

Then, the analysis continues as in Section 2.4. Namely, we compute for every signal  $\varphi_i$ , the approximate of the *first order derivative* of the map (1).

Patient 1 presents a focal seizure that generalizes. Figure 12 (top) shows a first peak only at Channel 0, where the seizure starts, and then the derivative associated to rest of the channels starts to increase. In the same direction, the derivative of some channels, like Channel 4 and Channel 5, remains higher for a longer period of time given the persistence of the seizure dynamics on those signals. On the contrary, Patient 3 presents a generalized seizure. Figure 12 (bottom) shows a consistent behavior of the all the channel during the entire ictal state.

#### 4. CONCLUSIONS

We have presented a novel approach with roots in algebraic topology to detect epileptic seizures in real time from neurophysiological recordings. Most standard techniques, like time-frequency analysis or complexity measures, rely in the (averaged) properties of the set of time series. On the contrary, our indicators works with the dynamic information provided by the whole set of signals. Indeed, we identify the ictal state in terms of the

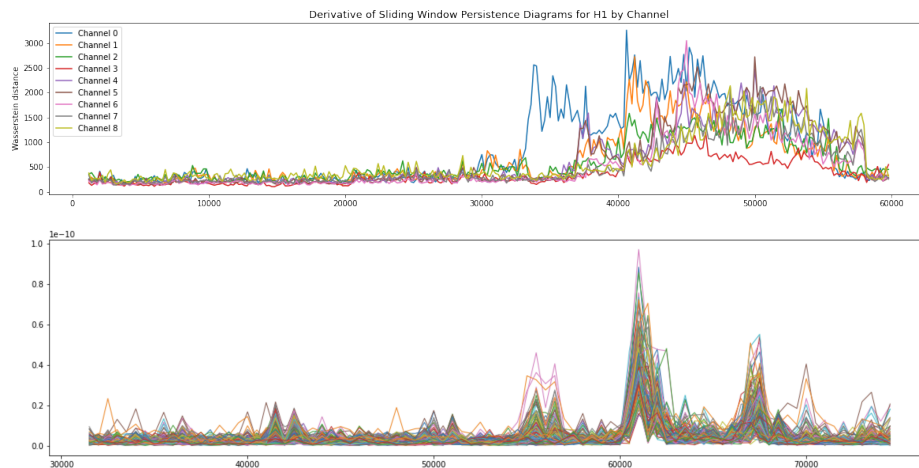


FIGURE 12. **Derivative biomarker for the persistence diagrams of the sliding-window time-delay embeddings.** **Top.** Patient 1. There are salient peaks only in the channels associated to the focal seizure at the beginning and end of the ictal state. **Bottom.** Patient 3. There are synchronized peaks at the start and end of the seizure for all the channels.

changes in the geometry of the embeddings produced by the geometric change in the dynamics. The topological nature of our point of view provides consistency to different methods of collection of the neural information, such as EEG, iEEG and MEG, and to a range of clinical conditions.

**Acknowledgements.** We are grateful to Eugenio Borghini for many useful discussions and suggestions during the preparation of this article. X. F. is a member of the Centre for Topological Data Analysis funded by the EPSRC grant EP/R018472/1. D. M. wants to thank for the financial support from MinCyT-FonCyT PICT-2019, N° 01750 PMO BID. For the purpose of Open Access, the authors have applied a CC BY public copyright licence to any Author Accepted Manuscript (AAM) version arising from this submission.

#### REFERENCES

- [1] Henry D. I. Abarbanel. *Analysis of observed chaotic data*. Institute for Nonlinear Science. Springer-Verlag, New York, 1996.
- [2] Henry D. I. Abarbanel, Reggie Brown, John J. Sidorowich, and Lev Sh. Tsimring. The analysis of observed chaotic data in physical systems. *Rev. Modern Phys.*, 65(4):1331–1392, 1993.
- [3] C. Bandt and B. Pompe. Permutation entropy: a natural complexity measure for time series. *Physical Review Letters*, 88(17):174102, 2002.
- [4] Ulrich Bauer. Ripser: efficient computation of Vietoris-Rips persistence barcodes. *J. Appl. Comput. Topol.*, 5(3):391–423, 2021.
- [5] Joan S. Birman and R. F. Williams. Knotted periodic orbits in dynamical systems. I. Lorenz’s equations. *Topology*, 22(1):47–82, 1983.
- [6] David Cohen-Steiner, Herbert Edelsbrunner, and John Harer. Stability of persistence diagrams. In *Proceedings of the twenty-first annual symposium on Computational geometry*, pages 263–271, 2005.
- [7] David Cohen-Steiner, Herbert Edelsbrunner, John Harer, and Yuriy Mileyko. Lipschitz functions have  $L_p$ -stable persistence. *Found. Comput. Math.*, 10(2):127–139, 2010.
- [8] Alex Cole, Gregory J. Loges, and Gary Shiu. Quantitative and interpretable order parameters for phase transitions from persistent homology. *Physical Review B*, 104(10):104426, 2021.

- [9] Don Coppersmith and Shmuel Winograd. Matrix multiplication via arithmetic progressions. In *Proceedings of the nineteenth annual ACM symposium on Theory of computing*, pages 1–6, 1987.
- [10] Luis Garcia Dominguez, Richard A Wennberg, William Gaetz, Douglas Cheyne, O Carter Snead, and Jose Luis Perez Velazquez. Enhanced synchrony in epileptiform activity? local versus distant phase synchronization in generalized seizures. *Journal of neuroscience*, 25(35):8077–8084, 2005.
- [11] Herbert Edelsbrunner and John L. Harer. *Computational topology*. American Mathematical Society, Providence, RI, 2010. An introduction.
- [12] Herbert Edelsbrunner, David Letscher, and Afra Zomorodian. Topological persistence and simplification. *Discrete Comput. Geom.*, 28(4):511–533, 2002. Discrete and computational geometry and graph drawing (Columbia, SC, 2001).
- [13] Ximena Fernandez, Eugenio Borghini, Gabriel Mindlin, and Pablo Groisman. Intrinsic persistent homology via density-based metric learning, 2020.
- [14] Robert Ghrist. Barcodes: the persistent topology of data. *Bull. Amer. Math. Soc. (N.S.)*, 45(1):61–75, 2008.
- [15] Robert Gilmore and Marc Lefranc. *The topology of chaos*. Wiley-Interscience [John Wiley & Sons], New York, 2002. Alice in Stretch and Squeezeland.
- [16] Barbara Giunti, Guillaume Houry, and Michael Kerber. Average complexity of matrix reduction for clique filtrations. *arXiv preprint arXiv:2111.02125*, 2022.
- [17] Ary Goldberger, Luís Amaral, L. Glass, Shlomo Havlin, J. Hausdorg, Plamen Ivanov, R. Mark, J. Mietus, G. Moody, Chung-Kang Peng, H. Stanley, and Physiokit Physiobank. Components of a new research resource for complex physiologic signals. *PhysioNet*, 101, 01 2000.
- [18] Hossein Sohanian Haghghi and Amir Hossein Davaie Markazi. A new description of epileptic seizures based on dynamic analysis of a thalamocortical model. *Scientific Reports*, 7, 2017.
- [19] Allen Hatcher. *Algebraic topology*. Cambridge University Press, Cambridge, 2002.
- [20] Alan L Hodgkin and Andrew F Huxley. A quantitative description of membrane current and its application to conduction and excitation in nerve. *The Journal of physiology*, 117(4):500, 1952.
- [21] Viktor K. Jirsa, William C. Stacey, Pascale P. Quilichini, Anton I. Ivanov, and Christophe Bernard. On the nature of seizure dynamics. *Brain*, 137(8):2210–2230, 06 2014.
- [22] Harold W Kuhn. The Hungarian method for the assignment problem. *Naval research logistics quarterly*, 2(1-2):83–97, 1955.
- [23] Yongjin Lee, Senja D Barthel, Paweł Dłotko, S Mohamad Moosavi, Kathryn Hess, and Berend Smit. Quantifying similarity of pore-geometry in nanoporous materials. *Nature communications*, 8(1):1–8, 2017.
- [24] Abraham Lempel and Jacob Ziv. On the complexity of finite sequences. *IEEE Transactions on information theory*, 22(1):75–81, 1976.
- [25] Emanuela Merelli, Marco Piangerelli, Matteo Rucco, and Daniele Toller. A topological approach for multivariate time series characterization: the epileptic brain. In *Proceedings of the 9th EAI international conference on bio-inspired information and communications technologies (formerly BIONET-ICS)*, pages 201–204, 2016.
- [26] Nikola Milosavljević, Dmitriy Morozov, and Primoz Skraba. Zigzag persistent homology in matrix multiplication time. In *Proceedings of the Twenty-Seventh Annual Symposium on Computational Geometry*, SoCG '11, page 216–225, New York, NY, USA, 2011. Association for Computing Machinery.
- [27] Dmitriy Morozov. Persistence algorithm takes cubic time in worst case. *BioGeometry News, Dept. Comput. Sci., Duke Univ*, 2, 2005.
- [28] Monica Nicolau, Arnold J Levine, and Gunnar Carlsson. Topology based data analysis identifies a subgroup of breast cancers with a unique mutational profile and excellent survival. *Proceedings of the National Academy of Sciences*, 108(17):7265–7270, 2011.
- [29] World Health Organization. Fact sheet on epilepsy. *Online*, 2022.
- [30] Nina Otter, Mason A Porter, Ulrike Tillmann, Peter Grindrod, and Heather A Harrington. A roadmap for the computation of persistent homology. *EPJ Data Science*, 6:1–38, 2017.
- [31] Yash Paul. Various epileptic seizure detection techniques using biomedical signals: a review. *Brain informatics*, 5(2):1–19, 2018.
- [32] Jose A. Perea. Topological times series analysis. *Notices Amer. Math. Soc.*, 66(5):686–694, 2019.
- [33] Jose A. Perea and John Harer. Sliding windows and persistence: an application of topological methods to signal analysis. *Found. Comput. Math.*, 15(3):799–838, 2015.

- [34] Piero Perucca, François Dubeau, and Jean Gotman. Intracranial electroencephalographic seizure-onset patterns: effect of underlying pathology. *Brain*, 137(1):183–196, 10 2013.
- [35] Arthur A. B. Pessa and Haroldo V. Ribeiro. ordpy: A Python package for data analysis with permutation entropy and ordinal network methods. *Chaos: An Interdisciplinary Journal of Nonlinear Science*, 31(6):063110, 2021.
- [36] Marco Piangerelli, Matteo Rucco, Luca Tesei, and Emanuela Merelli. Topological classifier for detecting the emergence of epileptic seizures. *BMC research notes*, 11(1):1–7, 2018.
- [37] Raúl Rabadán and Andrew J. Blumberg. *Topological data analysis for genomics and evolution: topology in biology*. Cambridge University Press, 2019.
- [38] N. Radhakrishnan and B.N. Gangadhar. Estimating regularity in epileptic seizure time-series data. *IEEE engineering in medicine and biology magazine*, 17(3):89–94, 1998.
- [39] Michael M. Schartner, Robin L. Carhart-Harris, Adam B. Barrett, Anil K. Seth, and Suresh D. Muthukumaraswamy. Increased spontaneous MEG signal diversity for psychoactive doses of ketamine, LSD and psilocybin. *Scientific reports*, 7(1):1–12, 2017.
- [40] Primoz Skraba and Katharine Turner. Wasserstein stability for persistence diagrams, 2020.
- [41] Stephen Smale. Differentiable dynamical systems. *Bulletin of the American mathematical Society*, 73(6):747–817, 1967.
- [42] Floris Takens. Detecting strange attractors in turbulence. In *Dynamical systems and turbulence, Warwick 1980 (Coventry, 1979/1980)*, volume 898 of *Lecture Notes in Math.*, pages 366–381. Springer, Berlin-New York, 1981.
- [43] Alexandros T. Tzallas, Markos G. Tsipouras, Dimitrios G. Tsalikakis, Evaggelos C. Karvounis, Loukas Astrakas, Spiros Konitsiotis, and Margaret Tzaphlidou. Automated epileptic seizure detection methods: a review study. *Epilepsy–Histological, Electroencephalographic and Psychological Aspects*, pages 2027–2036, 2012.
- [44] José Luis Perez Velazquez, Luis Garcia Dominguez, Vera Nenadovic, and Richard A Wennberg. Experimental observation of increased fluctuations in an order parameter before epochs of extended brain synchronization. *Journal of biological physics*, 37(1):141–152, 2011.
- [45] Robert F. Williams. Expanding attractors. *Publications Mathématiques de l’IHÉS*, 43:169–203, 1974.
- [46] Yuan Yao, Jian Sun, Xuhui Huang, Gregory R. Bowman, Gurjeet Singh, Michael Lesnick, Leonidas J. Guibas, Vijay S. Pande, and Gunnar Carlsson. Topological methods for exploring low-density states in biomolecular folding pathways. *The Journal of chemical physics*, 130(14):04B614, 2009.
- [47] X-S Zhang, Rob J. Roy, and Erik W. Jensen. EEG complexity as a measure of depth of anesthesia for patients. *IEEE transactions on biomedical engineering*, 48(12):1424–1433, 2001.
- [48] Mengni Zhou, Cheng Tian, Rui Cao, Bin Wang, Yan Niu, Ting Hu, Hao Guo, and Jie Xiang. Epileptic seizure detection based on EEG signals and CNN. *Frontiers in neuroinformatics*, 12:95, 2018.

DEPARTMENT OF MATHEMATICAL SCIENCES, DURHAM UNIVERSITY, UNITED KINGDOM.  
 Email address: ximena.l.fernandez@durham.ac.uk

UNIVERSIDAD AUTÓNOMA DE ENTRE RÍOS (UADER) AND INSTITUTO DE MATEMÁTICA APLICADA DEL LITORAL (IMAL-CONICET-UNL), ARGENTINA.  
 Email address: dmateos@santafe-conicet.gov.ar